Hindawi
Advances in Polymer Technology
Volume 2020, Article ID 8855577, 12 pages
https://doi.org/10.1155/2020/8855577

Research Article

Development and Performance Evaluation of Cellulose Acetate-Bentonite Mixed Matrix Membranes for CO_2 Separation

Asif Jamil,[1] Momina Zulfiqar,[1] Usama Arshad,[1] Subhan Mahmood,[1] Tanveer Iqbal,[1] Sikander Rafiq,[1] and Muhammad Z. Iqbal[2]

[1]*Department of Chemical, Polymer and Composite Materials Engineering, University of Engineering and Technology Lahore (New Campus), Lahore, Pakistan*
[2]*Department of Chemical and Petroleum Engineering, United Arab Emirates University (UAEU), PO Box 15551, Al Ain, UAE*

Correspondence should be addressed to Sikander Rafiq; sikanderafiq@gmail.com

Received 14 September 2020; Revised 27 November 2020; Accepted 2 December 2020; Published 14 December 2020

Academic Editor: Lucia Baldino

Membrane science is a state-of-the-art environmentally green technology that ascertains superior advantages over traditional counterparts for CO_2 capture and separation. In this research, mixed matrix membranes (MMMs) comprising cellulose acetate (CA) with various loadings of bentonite (Bt) clay were fabricated by adopting the phase-inversion technique for CO_2/CH_4 and CO_2/N_2 separation. The developed pristine and MMMs were characterized for morphological, thermal, structural, and mechanical analyses. Several techniques such as scanning electron microscopy, thermogravimetric analysis, Fourier transformed infrared spectroscopy, and nano-indentation investigations revealed the promising effect of Bt clay in MMMs as compared to pristine CA membrane. Nano-indentation test identified that elastic modulus and hardness of the MMM with 1 wt. loading was increased by 64% and 200%, respectively, compared to the pristine membrane. The permeability decreased with the incorporation of Bt clay due to uniform dispersion of filler attributed to enhanced tortuosity for the gas molecules. Nevertheless, an increase in gas separation performance was observed with Bt addition up to 1 wt. loading. The opposite trend prevailed with increasing Bt concentration on the separation performance owing to filler agglomeration and voids creation. The maximum value of ideal selectivity (CO_2/CH_4) was achieved at 2 bar pressure with 1 wt. % Bt loading, which is 79% higher than the pristine CA membrane. For CO_2/N_2, the ideal selectivity was 123% higher compared to the pristine membrane with 1 wt. % Bt loading at 4 bar pressure.

1. Introduction

Nowadays, it is widely conceded and understood that CO_2 emission is the pivotal reason behind climate changes, ocean acidification, and associated global warming. Among greenhouse gases, CO_2 exhibits the most dominating role, and its anthropogenic emission results in intensifying the greenhouse effect and climate change up to 64% [1]. The CO_2 emissions in atmosphere, majorly associated with combustion activities related to fossil fuels and industrial flue gases, have increased to 61% between 1990 and 2013 [2]. Therefore, CO_2 separation is inevitable, and efforts are underway at limited scale compared to what is required.

Currently, several techniques such as absorption, cryogenic distillation, and adsorption are used frequently to separate and capture CO_2 gas. Nonetheless, the aforementioned traditional techniques have shown certain drawbacks particularly in terms of capital cost, operational complications, and limited CO_2 loading capabilities [3]. Therefore, there is a need to look for low cost, environmentally benign, high loading capacity, and easily applicable CO_2 capturing technology. Membrane technology has the potential to offer superior advantages compared to the traditionally available technologies [4]. Membrane technology not only offers lower capital cost but also the design and operational simplicity, compactness, and energy efficiency along with environmentally friendliness are associated benefits [5, 6].

Membranes are developed either from inorganic or/and polymeric materials. However, combining both aforementioned materials proved to be advantageous with regard to membrane manufacturing cost and chemical and thermal stability as well as ease in processing [4, 7]. The fabrication of mixed matrix membrane (MMMs) with flawless or least affected morphology is strenuous and challenging and depends on the choice of materials [8]. Subsequently, inappropriate selection of materials may lead to interfacial defects and seriously damage the separation capacity of MMMs. Therefore, successful membrane formation is subject to the selection of compatible polymer filler systems. Generally, polysulfone (PSf), polyethersulfone (PES), polyimides (PI), and cellulose acetate (CA) are commonly used polymers for membrane fabrication [9–13]. CA offers inexpensive manufacturing, adequate toughness and virtuous compatibility, superior fouling resistance, easy processing, and high CO_2 solubility [14].

Clay minerals are characterized as earthy, fine-grained natural soil materials, and extensively studied as inorganic filler in polymer composite industry [15]. Montmorillonite (Mt) is a frequently used clay for reinforcing polymers among others such as cloisite and kaolin clays which are also used in manufacturing polymer composites [16, 17]. Bentonite is mostly Mt comprised of aluminum 2 : 1 phyllosilicate. The elementary structure of Mt unit cell comprised of a tetrahedral sheet containing silicon encircles by four oxygen atoms and an octahedral layer of aluminum surrounded by eight oxygen atoms [18]. The interactions of the organic polymer and clay particles dictate the morphology of the nanocomposites that could either be phase-separated, intercalated, and exfoliated as depicted in Figure 1. Exfoliated morphology is the most desired one and offers uniform distribution that promotes gas separation performance in MMM [19, 20].

CA is extensively studied as organic phase for polymeric and nano-composite gas separation membranes; however, its potential with bentonite clay incorporation is barely reported. Thus, in the present study, bentonite MMMs are fabricated, and the effect of Bt loading on the performance of CA-Bt MMMs is presented. Afterward, the fabricated MMMs are characterized by structural, morphological, thermal, and mechanical properties. Subsequently, gas separation (CO_2/N_2 and CO_2/CH_4) study was performed for the developed membranes.

2. Experimental

2.1. Materials. Cellulose acetate (CA, M_n 30,000) and tetrahydrofuran (THF, ≥99.5%) were purchased from Sigma-Aldrich. Bentonite clay was provided by Marshal trading company, Pakistan, and was used as received.

2.2. Optimization of CA Concentration. The defect-free membrane morphology is subject to the dissolution of optimized polymer concentration in solvent. Therefore, five dope-solutions with varying CA concentration (5, 10, 15, and 20 wt. %) in THF were prepared at ambient conditions. The dope-solution was left for stirring for 24 hours to completely dissolve CA in THF, followed by degassing for another 24 hours to eliminate any entrapped air bubbles. The viscosities of the degassed solutions were determined using rheometer by measuring the viscosity change against the time, whilst all other parameters were kept constant.

2.3. Dope-Solution Preparation. Prior to preparing the dope-solution, CA was dried overnight at 100°C to remove the moisture content, whereas THF and bentonite were used as received. The dried CA was dissolved in THF to formulate 13% *w*/*w* polymer solution and fabricate the pristine polymeric membrane.

For MMM, the desired 0.5 wt. % Bt was dispersed in THF by stirring for 60 minutes to ensure uniform dispersion at room temperature. A 5 wt. % of CA solution was added in the dispersed mixture for priming purposes and magnetically stirred for 3 hours. The remaining amount of CA was poured gradually to get complete polymer dissolution whilst keeping stirring rate of 650 rpm for 24 hours. Subsequently, the prepared CA-Bt solution was allowed to degas for 12 hours at ambient conditions. A similar procedure was repeated to synthesize the rest of MMMs. The synthesized pristine and MMMs comprised of 0.5 wt. %, 1 wt. %, 1.5 wt. %, and 2 wt. % loading of bentonite are coded as M1, M2, M3, M4, and M5, respectively.

2.4. Membrane Development. The CA-Bt MMMs were fabricated through the dry-wet phase inversion technique. The tape casting unit with adjustable film thickness was used, and the casted membranes were kept at ambient temperature for 24 hours prior to immersion in distilled water for a day to encounter solvent exchange. The developed pristine and MMMs were dried in a vacuum oven in order to evaporate the residual solvent at 70°C for 12 hours.

2.5. Characterization of the Developed Pristine and MMMs. The dry-wet phase inversion method was adopted to fabricate CA-Bt MMMs, and this influenced the membrane structure. Therefore, the morphology of the casted membranes was studied through SEM analysis.

The possible functional groups attached to the developed membranes were identified by FTIR spectroscopy (Perkin Elmer 1650). The spectra of all the membranes were obtained in the range of 400 to 4000 cm^{-1} under the transmission mode.

TGA (Perkin Elmer, STA6000) was used to determine the thermal stability of CA-Bt MMMs. The thermal behavior was analyzed in the presence of nitrogen environment by using a heating rate of 10°C/min for a temperature range of 30 to 800°C.

2.6. Pure Gas Permeation Test. The permeation behavior of developed MMMs was evaluated by using pure N_2, CO_2, and CH_4 gases at ambient temperature, whilst at varied pressure from 2 to 6 bars. Prior to carry out permeation tests, the system was evacuated from air gases by using vacuum pump. The flow rate of the membrane permeated gases was measured by using soap bubble flowmeter. This can be done simply by recording the time taken by the bubble to move from zero to a certain higher level

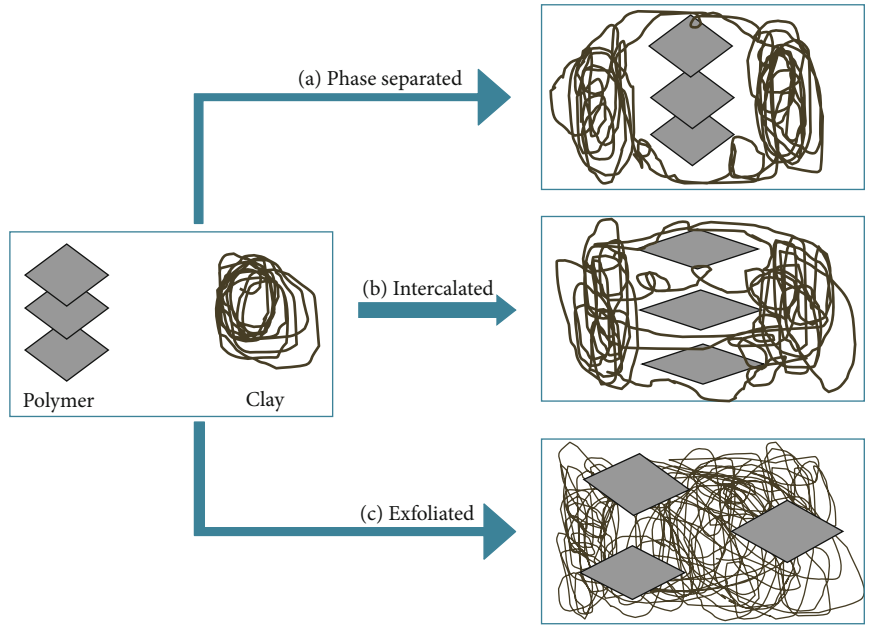

Figure 1: Clay dispersion morphology: (a) phase separated, (b) intercalated, and (c) exfoliated.

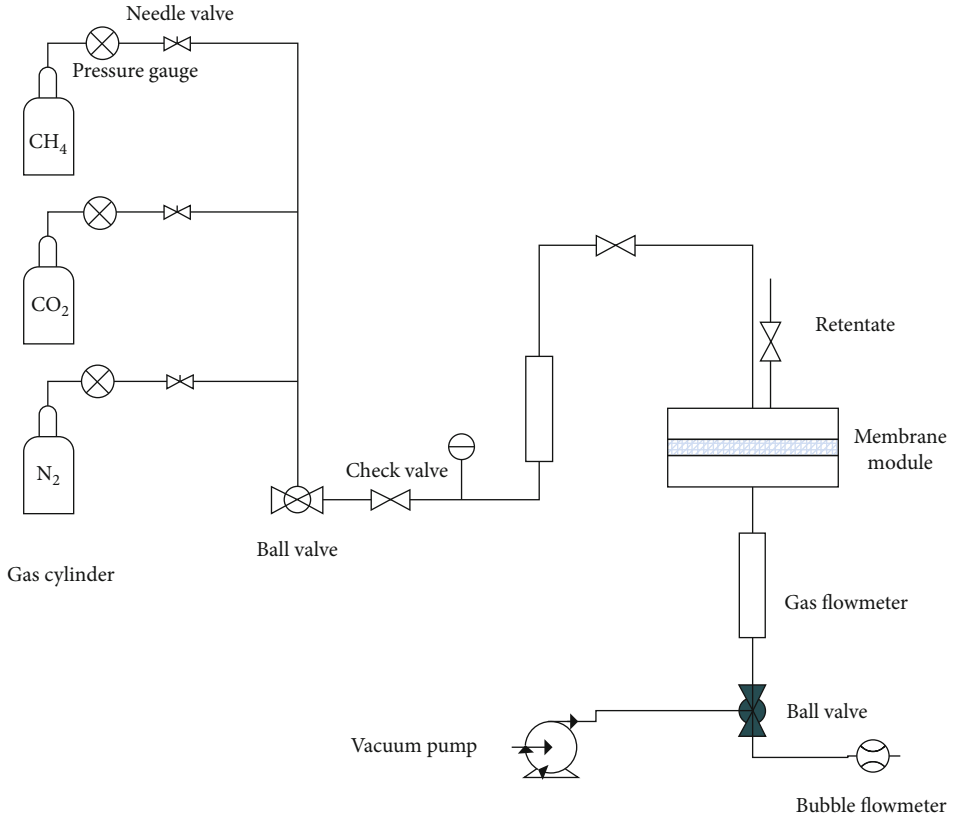

Figure 2: Schematic diagram of gas permeation rig.

[21]. Figure 2 presents the schematic diagram of the gas permeation rig used in this study.

The standard equations (1) and (2) as provided are used to calculate the permeability and selectivity of the permeated gases, respectively [15].

$$P_a = \frac{Ql}{A\Delta P}\frac{273.15}{T}, \tag{1}$$

$$\alpha_{ab} = \frac{P_a}{P_b}, \tag{2}$$

where P_a is the gas permeability (barrer), Q represents the volumetric flow rate (cm^3/s), l is the membrane thickness, A corresponds to effective surface area (cm^2), ΔP is the transmembrane pressure (cm.Hg), and T is the temperature (K). On the other hand, selectivity is represented by α_{ab} for gas a to b.

2.7. Mechanical Analysis Using Nano-Indentation Technique. The nano-indentation test was performed by adopting continuous stiffness measurement technique. The aforementioned test records the displacement of pyramidal diamond at the sample surface produced by a dynamic load. The test in this study was carried out with load of indentation around 100 mN and applied at least at 38 points on each mixed matrix membrane. The nano-indentation permits measuring the mechanical properties, hardness, and reduced Young's modulus of thin membranes. The schematic diagram of studied membrane is shown in Figure 3.

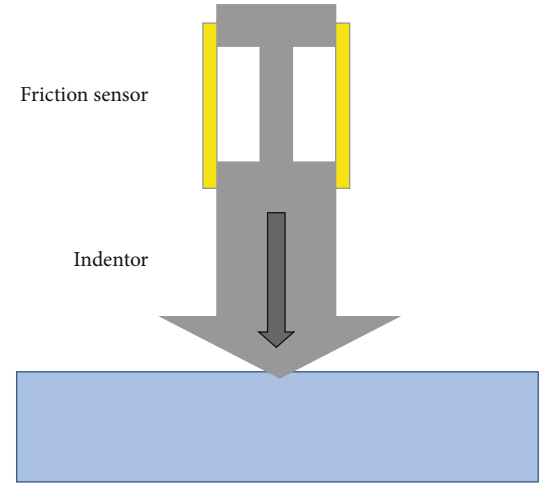

Figure 3: Schematic diagram of nano-indentation test on the membrane sample.

3. Results and Discussion

3.1. Optimization of CA Concentration. Figure 4 presents the viscosity curve for a binary dope solution comprised of 5 to 20 wt. % CA in THF solvent. An upward trend in the viscosity curve is observed with increase in CA composition in dope solution. Initially, the viscosity increased gradually with CA concentration. Nonetheless, the curve becomes steeper beyond a critical polymer concentration. This critical polymer concertation can be found by extrapolating the linear sections of the curve and then intercepting at a point as shown in Figure 4. This method of determining critical polymer concentration from the viscosity curve has been used frequently and regarded as a valid approach in membrane development technique [22].

The aforementioned method was used here, and critical dope viscosity was determined at 13 wt. % CA concentration. The critical dope viscosity is associated with the polymer chain entanglements at a particular polymer concentration in dope solution. Below this critical dope viscosity point, polymer chains exhibit loose packing and hence welcome the intrusion of nonsolvent to create voids at the surface. The membrane formation with the dope solution below critical polymer concentration forms porous morphology with weak mechanical properties. In the contrary, above the critical dope viscosity, polymer chains demonstrate remarkable entanglements that impede nonsolvent diffusion through the surface forming dense, void-free structure. The membrane formation above critical dope viscosity produces nonporous and mechanically strong morphology [23]. Therefore, it is important to know the critical viscosity of polymer solutions since it a balance between highly dense and porous structures in membranes to achieve optimum separation performance [22].

3.2. Chemical Analysis. FTIR was used to analyze the characteristic peaks appeared in Bt, pure CA, and CA-Bt MMM spectra and are depicted in Figure 5. The spectrum of Bt nanoparticles exhibits a characteristic bands at 1043, 1713, and 2850 cm^{-1} and is associated with Al-O-Si deformation, carbonyl groups stretching, and C-H bonding stretching [1].

For the developed membranes, the peaks appearing below 900 cm^{-1} represent C-O vibrations in alcohols which might be due to the presence of residual THF in the membrane [23]. The peak at 901 cm^{-1} is attributed to the β-links in the pristine CA membrane [24]. On the other hand, bands at 1033 cm^{-1}, 1124, and 1159 cm^{-1} are attributed to symmetric and asymmetric C-O vibrations in secondary alcohol [3]. The bands observed at 1218 cm^{-1}, 1367 cm^{-1}, and 1437 cm^{-1} correspond to C-C-O stretching, CH_3 deformation, and H-C-H vibrations, respectively [25]. The characteristic C=O stretching vibration in CA was observed at 1733 cm^{-1} [25]. Similarly, the peak observed around 3000 cm^{-1} represents the mild effects of carboxylic acid [26]. These observations signify the presence of CA-Bt interactions in the synthesized membrane structures.

3.3. Morphological Analysis. Gas transport properties across the MMM strongly depend on the structural morphology of resultant membranes. SEM was used to analyze the morphology and structure of the pure CA membrane and MMMs, as well as the interfacial interactions of the CA and Bt particles. Figure 6 shows the cryo-fractured membrane cross-sections. Generally, clay particles owing to small size are invisible in SEM images unless form agglomerates.

Furthermore, the synthesized membranes exhibited dense morphology with the presence of certain voids. For gas separation membranes, the dense morphology is always preferred as it provides superior separation performance compared to its counterpart porous morphology [27]. The membrane (M2) showed dense morphology with fewer voids, which are attributed to the evaporation of THF traces during membrane drying. M3 membrane presented the uniform dense and voids free morphology. These observations anticipate the uniform Bt dispersion in CA, which ascertained dense, voids free membrane

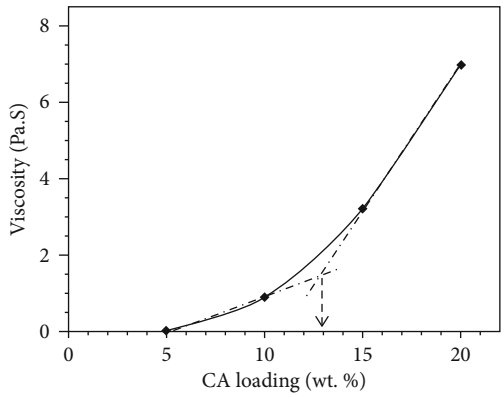

Figure 4: Critical concentration evaluation of CA in THF.

morphology. For M4 and M5 membranes, clay agglomeration led to the increased void formation, which consequently decreases the separation performance of these membranes. It is also observed that the void size and void frequency increase with increasing clay loading. The aforementioned observations are in agreement with previously reported studies on the clay agglomeration in the polymer matrix [15, 17, 28].

3.4. Thermal Stability Analysis. The thermal stability of pristine CA and CA-Bt MMMs at various Bt loadings is shown in Figure 7. For simplicity, the decomposition temperature is considered at 10% weight loss. The thermogram showed no weight loss below 200°C, which is attributed to complete solvent removal from the synthesized membranes.

The decomposition temperature for the pristine CA membrane is 235.27°C. The thermal stability increased with the addition of Bt. This improvement is attributed to the inherent thermal characteristics of Bt, as the latter absorbed the greater amount of heat. In addition, nano-fillers settle in the polymer chains and impede the interchain segmental motion, which consequently, enhance the energy needed for polymer chain movement [29]. In comparison to pristine membrane, the addition of 0.5, 1, 1.5, and 2 wt. % Bt increased the decomposition temperature to 290.14, 244.41, 243.52, and 240.76°C, respectively. Among composite membranes, the maximum thermal stability achieved is with 0.5 wt. % clay, which is attributed by the uniform dispersion of the clay platelets.

A similar trend was observed by Liang in montmorillonite (Mt) filled PES membranes [28]. The addition of Mt (2 to 20 wt. %) consistently improved the thermal stability of the MMMs. Herrra-Alonso also observed similar findings with Cloisite Na^+ in PBMA where the onset degradation temperature increased from 222 to 260°C with the addition of clay (0-5 wt. %) [30]. PMMA/clay nanocomposite also showed similar trend; thermal stability improved owing to the higher content of alumino-silicate in Mt. The improvement in decomposition temperature is due to layered morphology of clay which restricted the oxygen gas' diffusion into polymer phase. The heat provided is absorbed by the clay platelets, eventually delaying the decomposition process [31].

3.5. Nano-Indentation Analysis

3.5.1. Load Displacement Curves. The average penetration depth at peak load for the loading-unloading cycle for the pristine membrane is 195 μm. With the introduction of clay in 0.5 wt. % loading, the displacement depth decreases to approximately 145 μm, which is about 25% lower than the pristine CA membrane. The decreasing trend continued until 1.5 wt. % Bt loading due to the increase in impermeable stiffer clay platelets. Nevertheless, at higher bentonite loading (2 wt. %), the indentation depth of MMM is decreased to 26% lower than the pristine CA membrane. The degree of the dispersion of clay might increase the resistance to plastic deformation contributing to a lower depth of indentation.

A constant load of 100 mN was applied on the membrane samples, and unloading of this force imparts creep region as shown by hysteresis in Figure 8. Creep is the change in depth overtime where the force is kept constant, and a new limit is reached immediately beforehand. After that creeping area, the indenter starts to unload. As the unloading curves do not overlap with the loading curves, it implies that the developed membranes are not completely elastic but also shows plastic behavior [32]. For all the developed membranes, the loading and unloading curves appeared to be uninterrupted and stable [33].

3.5.2. Indentation Hardness. The indentation hardness (H) gauges the developed membranes' resistance against plastic or permanent deformation [34]. Theoretically, the hardness is an intrinsic property of materials and varies by the change in contact depth [35]. As anticipated, the addition of bentonite clay to cellulose acetate has a significant effect on nanohardness.

In general, the rise in clay loading greatly improved the membranes' mechanical properties [36]. It is noticed that hardness increases with the rise in bentonite composition in the developed membranes as depicted in Table 1. Hence, proper dispersion can cause the membrane to become harder and to resist the penetration of indenter into the sample. For M4 and M5 membranes, dramatic increase in hardness is observed. The clay particles agglomerated at this much loading as depicted in SEM micrographs; the nano-indenter might hitting the agglomerated area. Hence, an exponential increase in hardness is observed for membranes incorporating Bt loading beyond 1.5 wt. % loading.

3.5.3. Elastic Modulus. The elastic modulus of a particular membrane depends on the contact depth of the indenter and is presented in Table 1. The elastic modulus of the synthesized membranes decreases with increasing contact depth [32]. The elastic modulus increased linearly with increasing clay concentration in the CA matrix, which shows the brittle behavior of the MMMs. The presence of clay particles inside in CA chains makes them stiffer to resist chain orientation and imparts plasticity in the composite membrane. With an increase in clay concentration in MMMs, the modulus is higher than the pristine CA membrane, and therefore, MMM has more resistance to elastic deformation as stress is applied [32].

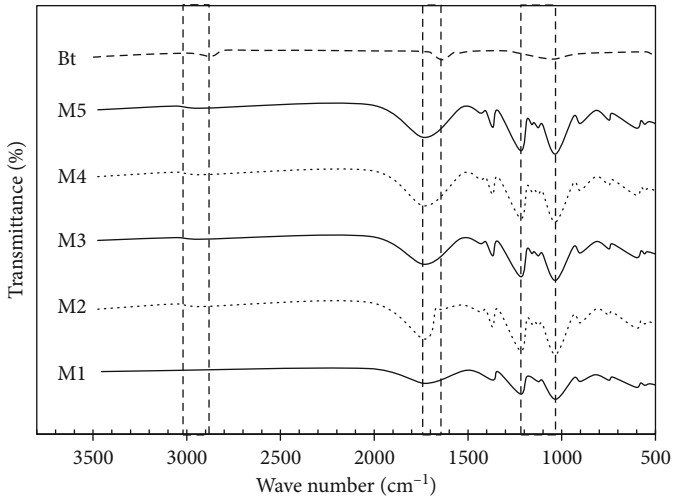

Figure 5: FTIR spectra of Bt, pristine, and MMMs.

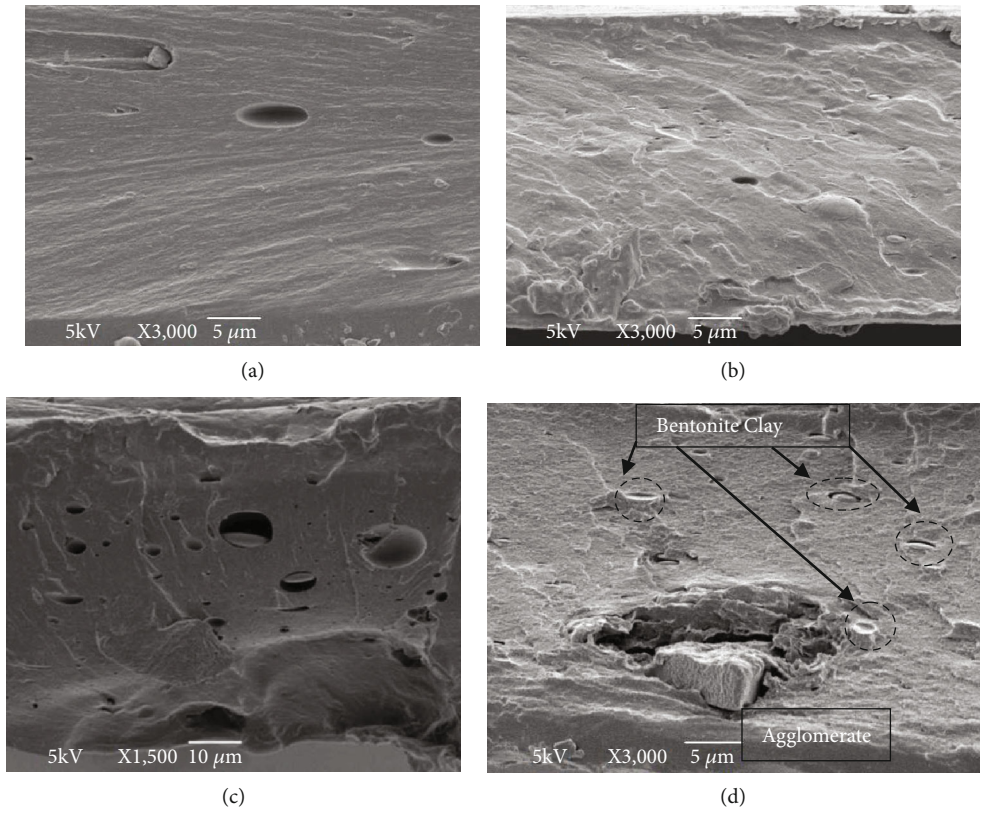

Figure 6: SEM micrographs of (a) M2, (b) M3, (c) M4, and (d) M5.

3.6. Gas Permeation Performance. The permeation of CO_2, N_2, and CH_4 gases in CA and CA/bentonite clay MMMs was investigated at room temperature. The gas permeation tests were carried out in a constant pressure setup at 2, 4, and 6 bar.

3.6.1. Effect of Feed Pressure on MMM Performance. Figure 9 represents the CO_2, CH_4, and N_2 permeability of the developed pristine and MMMs at various Bt loadings. For the pristine CA membrane, with increasing CO_2 feed pressure, the permeance decreased at all pressures. This attribute of CA is associated with its glassy nature as the stiff polymer chains as well as the pendant group of CA hamper the close chain packing and enhance the available free volume. Therefore, with the rise in incident gas pressure, the polymer chains shift from freely packed to closely packed structure, thereby suppress the available free volume and restrict the gas molecules diffusion through the membrane.

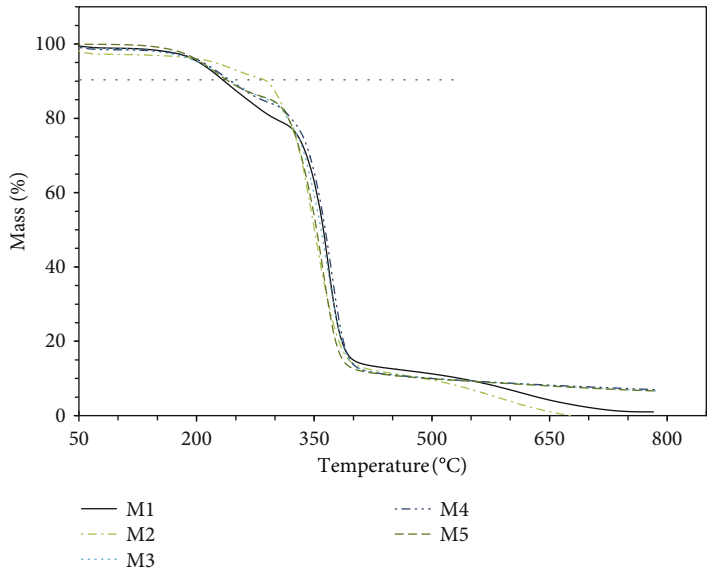

Figure 7: Thermogravimetric analysis of the developed membranes.

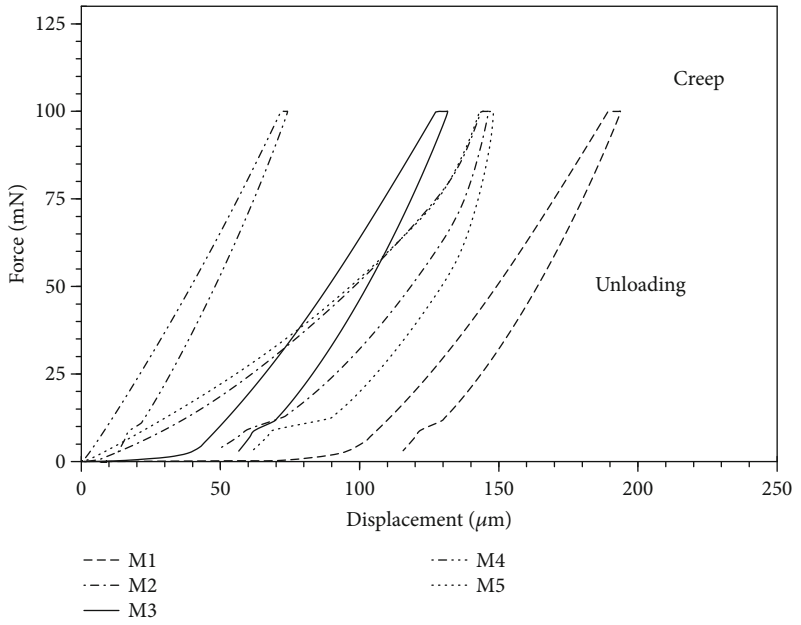

Figure 8: Load displacement curve of the developed membranes.

Table 1: Nano-indentation test results for developed membranes.

Sample	E-Modulus $\times 10^{-3}$ (GPa)	Max depth (μm)	Hardness $\times 10^{-4}$ (GPa)
M1	5.0	195	1.08
M2	6.3	145	3.41
M3	8.2	132	4.54
M4	13.0	74	119.37
M5	18.0	148	235.82

The dual-sorption model explains the sorption and diffusion of gas molecules through the polymer matrix and combined Henry's law and Langmuir behavior. The former defines the dissolution in the rubbery phase, whereas the latter explains the microvoids presence in glassy polymers [37]. CO_2 solubility increases initially with pressure according to Henry's Law; nevertheless, soon become constant and independent of pressure as the voids in glassy polymer start shrinking with further pressure increase due to Langmuir's behavior. Similarly, CH_4 and N_2 exhibited a similar downward trend with increasing pressure. This behavior of the gases is consistent with the previously published literature [38, 39].

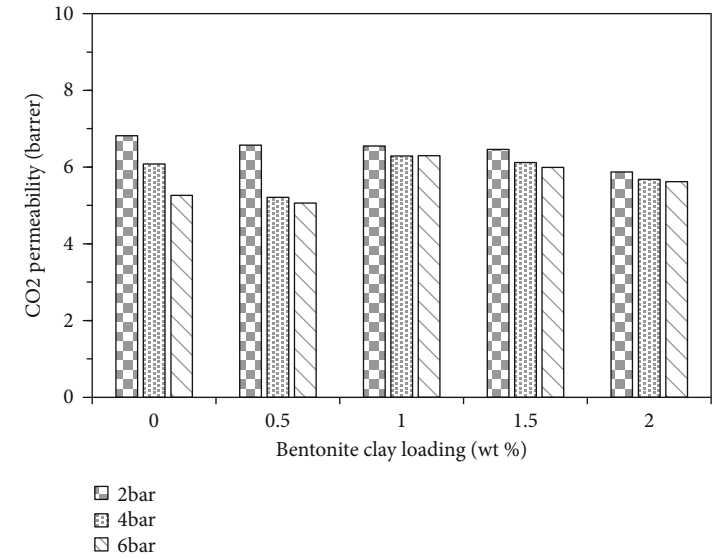

(a)

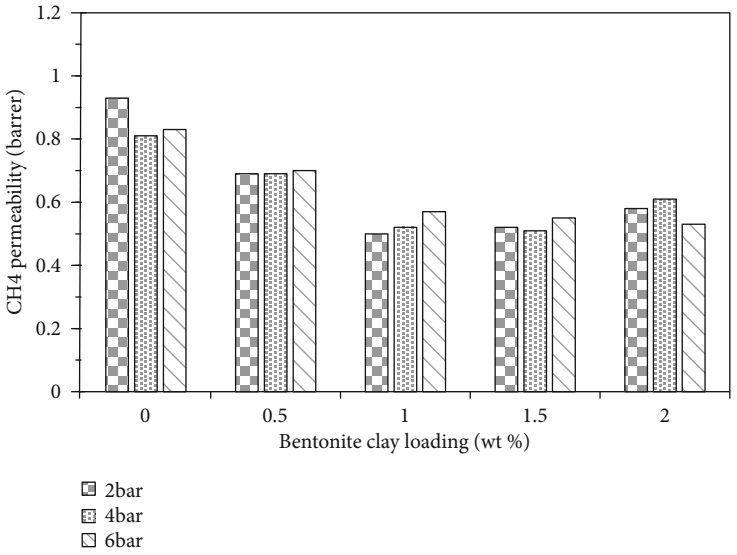

(b)

Figure 9: Continued.

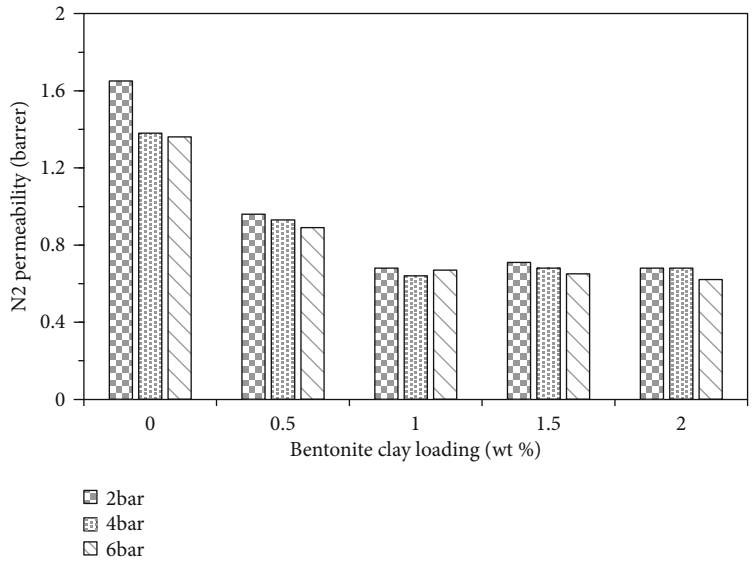

(c)

Figure 9: Gas permeability performance of developed membranes for (a) CO_2, (b) CH_4, and (c) N_2.

Moreover, the permeability of gases across membranes depends upon the solubility and diffusivity of the incident gas molecules. The former is a thermodynamic property and depends upon the gas condensability at the membrane surface, whereas latter depends upon the shape and size of the incident molecules [4, 40]. Figure 9 shows that CO_2 exhibited the highest permeability for pristine and MMMs compared to other gases at all pressure range. Since, CO_2 owing to its polar nature has higher condensability as well as solubility towards the glassy CA membrane compared to CH_4 and N_2 gases. Apart from solubility, the lower kinematic diameter and linear molecular shape of CO_2 compared to other counterparts are advantageous for fast diffusion across the CA membranes [41]. That is why the permeability of CO_2 gas is higher compared to CH_4 and N_2 gases across the developed pristine and MMMs. The permeability decreased in the following order: $CO_2 > CH_4 > N_2$. The decreasing trend is ascribed to the solubility difference and kinematic diameter of the gas molecules. It is also observed that the permeability of CH_4 and N_2 across developed membranes was not considerably affected by pressure changes from 2 to 6 bar. Maryam et al. developed Pebax-Clay MMMs and reported similar behavior for CH_4 and N_2 gases against incident gas pressure [42]. This is due to the fact that for most diffusion controlled incident gases, solubility and diffusion coefficient remain unaffected with increase in pressure [43, 44]. For instance, the incident gases with low-adsorbing and condensing attributes remain unchanged or slightly changed with increase in transmembrane pressure. The opposite trend is associated with the penetrants having high adsorption as well as condensation; the solubility and permeability coefficients exhibit soaring effect with an increase in pressure [43].

3.6.2. Effect of Bentonite on MMM Selectivity. Bentonite clay loading may influence the gas separation efficiency of MMMs; therefore, it is pondered as a one influential parameter in this analysis. Figure 9 shows the CO_2 permeance of the synthesized membrane with increasing filler concentration. It is observed that with the addition of bentonite, the permeability exhibited a decreasing trend at 2 bar pressure. This decreasing trend showed uniform distribution of bentonite clay in exfoliated morphology. These exfoliated clay particles act as impermeable phase and settle in polymer chains to restrict the gas diffusion pathways [45]. The aforementioned phenomenon is the reason of the permeation decrement in pristine and CA-Bt MMMs.

This decreasing trend with Bt addition is not limited to CO_2 only, but the trend is more prominent for CH_4 and N_2 gas. As mentioned earlier, diffusion is considered as the leading transport mechanism for CH_4 and N_2 gas across the membrane. Due to the higher kinematic diameter of N_2 (3.64 Å) and CH_4 (3.80 Å), the permeability is lower compared to CO_2 (3.30 Å) gas. Furthermore, since the bentonite clay particles are impermeable and stiff materials and its uniform disruption create tortuous path for the incident gas molecules and create obstruction of the large gas molecules to pass through [46].

Figures 10(a) and 10(b) present the ideal selectivity of CO_2/CH_4 and CO_2/N_2 at various Bt loadings. For the pristine CA membrane, the membranes at various bentonite clay loadings showed improved ideal selectivity. It is noted that the highest CO_2/CH_4 and CO_2/N_2 selectivity was noticed at all pressures for 1 wt. % bentonite clay. The ideal selectivity of CO_2/N_2 and CO_2/CH_4 selectivity increase from 4.13 and 7.33 to 6.15 and 9.07, respectively, at 2 bar.

An upward trend in the ideal selectivity of the membranes is prevailed until 1 wt. % Bt incorporation, which then reversed with further Bt addition for both CO_2/CH_4 and CO_2/N_2 selectivity. For CO_2/CH_4, the highest selectivity attained is 13.1 at 2 bar pressure, and this is 79% higher than pristine CA membranes. Moreover, the membrane with 1% loading displayed the maximum ideal selectivity (CO_2/N_2)

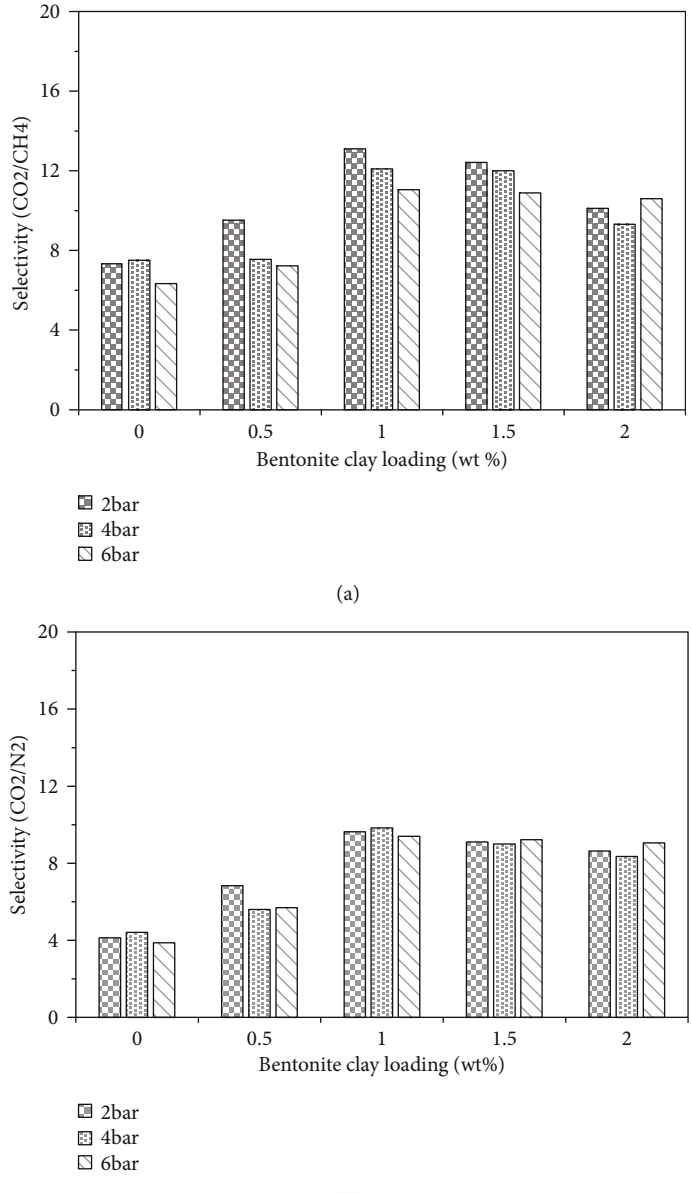

Figure 10: Ideal selectivity of (a) CO_2/CH_4 and (b) CO_2/N_2 for the developed membranes.

in comparison to pristine and MMMs at all transmembrane pressures. Nevertheless, the maximum selectivity noticed is 9.83 at 4 bar, which is 123% higher than pure CA membranes. Above this concentration, the filler started to form agglomerates; void morphology appeared and influenced the membrane surface and hampered the separation characteristics [47, 48]. Thus, any further increase beyond 1 wt. % loadings of clay particles do not significantly increase the CO_2/CH_4 and CO_2/N_2 selectivity of the developed MMMs. Therefore, it is concluded that the addition of Bt clay expands the gas separation performance of the MMMs compared. Hashemifard incorporated Cloisite 15 in the PEI matrix and observed similar results [16]. Ideal morphology existed below 2 wt. % of filler loading, upon which increment caused void morphology and deteriorate the MMM separation performance.

4. Conclusion

In this work, the potential of bentonite clay (Bt) as the inorganic filler has been investigated in cellulose acetate (CA) membranes. The phase-inversion technique was adopted for the fabrication of pristine CA membrane as well as MMMs with various Bt loadings in the CA matrix. The thermal stability of membranes improved with increasing Bt loading due to heat resistant properties of the clay particles. The load-displacement test showed that at 2% Bt loading, penetration depth decreases to 62% than that of the pristine membrane, which was further supported by the hardness test that showed a soaring trend with Bt incorporation. Furthermore, the improved elastic modulus of the developed membranes reflects the superior interfacial interactions of Bt in the CA system.

Gas separation tests of the developed membrane exhibited a remarkable increase in CO_2/CH_4 selectivity by the addition of Bt at constant pressure. Generally, the permeability of incident gases decreased for MMMs with reference to the pristine membrane by virtue of the tortuosity induced by the Bt platelets inside CA matrix. The MMMs at 1 wt. % Bt loading proved to be the most suitable composition and showed superior gas separation performance. Meanwhile, the ideal selectivity of CO_2/CH_4 and CO_2/N_2 has soared to 79% and 123%, respectively. Thus, it can be concluded that the Bt incorporation in the CA matrix has the potential to exhibit thermally, mechanically, and morphologically improved MMMs along with superior CO_2 separation characteristics.

Data Availability

The datasets generated during and/or analyzed during the current study are available from the corresponding author on reasonable request.

Conflicts of Interest

The authors declare that they have no conflicts of interest.

Acknowledgments

This research work was supported by the Department of Chemical, Polymer and Composite Materials Engineering, UET Lahore (New Campus), Pakistan. The authors would like to appreciate Mr. Muhammad Sulaiman for providing the technical assistance in carrying out nano-indentation testing of the membranes.

References

[1] A. E. Elkhalifah, S. Maitra, M. A. Bustam, and T. Murugesan, "Effects of exchanged ammonium cations on structure characteristics and CO_2 adsorption capacities of bentonite clay," *Applied Clay Science*, vol. 83, pp. 391–398, 2013.

[2] Z. Jahan, M. B. Niazi, M. B. Hägg, and W. Gregersen, "Decoupling the effect of membrane thickness and CNC concentration in PVA based nanocomposite membranes for CO_2/CH_4 separation," *Separation and Purification Technology*, vol. 204, pp. 220–225, 2018.

[3] M. Mubashir, Y. F. Yeong, K. K. Lau, T. L. Chew, and J. Norwahyu, "Efficient CO_2/N_2 and CO_2/CH_4 separation using NH2-MIL-53 (Al)/cellulose acetate (CA) mixed matrix membranes," *Separation and Purification Technology*, vol. 199, pp. 140–151, 2018.

[4] A. Jamil, O. P. Ching, and A. B. Shariff, "Current status and future prospect of polymer-layered silicate mixed-matrix membranes for CO2/CH4Separation," *Chemical Engineering & Technology*, vol. 39, no. 8, pp. 1393–1405, 2016.

[5] A. A. Olajire, "CO_2 capture and separation technologies for end-of-pipe applications–a review," *Energy*, vol. 35, no. 6, pp. 2610–2628, 2010.

[6] P. S. Goh, A. F. Ismail, S. M. Sanip, B. C. Ng, and M. Aziz, "Recent advances of inorganic fillers in mixed matrix membrane for gas separation," *Separation and Purification Technology*, vol. 81, no. 3, pp. 243–264, 2011.

[7] H. T. Afarani, M. Sadeghi, and A. Moheb, "The gas separation performance of polyurethane–zeolite mixed matrix membranes," *Advances in Polymer Technology*, vol. 37, no. 2, 348 pages, 2018.

[8] M. Mubashir, C. T. Leng, L. K. Keong, and N. Jusoh, "Study on the effect of process parameters on CO_2/CH_4 binary gas separation performance over NH_2-MIL-53 (Al)/cellulose acetate hollow fiber mixed matrix membrane," *Polymer Testing*, vol. 81, p. 106223, 2020.

[9] R. Ur Rehman, S. Rafiq, N. Muhammad et al., "Development of ethanolamine-based ionic liquid membranes for efficient CO2/CH4 separation," *Journal of Applied Polymer Science*, vol. 134, no. 44, 2017.

[10] D. Wang, K. Li, and W. K. Teo, "Polyethersulfone hollow fiber gas separation membranes prepared from NMP/alcohol solvent systems," *Journal of Membrane Science*, vol. 115, no. 1, pp. 85–108, 1996.

[11] X. Xu, J. Wang, J. Dong, H. B. Li, Q. Zhang, and X. Zhao, "Ionic polyimide membranes containing Tröger's base: synthesis, microstructure and potential application in CO_2 separation," *Journal of Membrane Science*, vol. 602, p. 117967, 2020.

[12] B. J. Sundell, D. J. Harrigan, S. C. Hayden et al., "Improved gas transport properties of cellulose acetate via sub-Tg acid-catalyzed silanation," *Journal of Membrane Science*, vol. 573, pp. 448–454, 2019.

[13] N. Gholami and H. Mahdavi, "Nanofiltration composite membranes of polyethersulfone and graphene oxide and sulfonated graphene oxide," *Advances in Polymer Technology*, vol. 37, no. 8, 3541 pages, 2018.

[14] M. Mubashir, Y. Y. Fong, C. T. Leng, and L. K. Keong, "Enhanced gases separation of cellulose acetate membrane using N-Methyl-1-2 pyrrolidone as fabrication solvent," *International Journal of Automotive and Mechanical Engineering*, vol. 15, no. 1, pp. 4978–4986, 2018.

[15] A. K. Zulhairun, A. F. Ismail, T. Matsuura, M. S. Abdullah, and A. Mustafa, "Asymmetric mixed matrix membrane incorporating organically modified clay particle for gas separation," *Chemical Engineering Journal*, vol. 241, pp. 495–503, 2014.

[16] S. A. Hashemifard, A. F. Ismail, and T. Matsuura, "Effects of montmorillonite nano-clay fillers on PEI mixed matrix membrane for CO_2 removal," *Chemical Engineering Journal*, vol. 170, no. 1, pp. 316–325, 2011.

[17] Y. Q. Gill, M. Song, and U. Abid, "Permeation characterization and modelling of polyethylene/clay nanocomposites for packaging," *Polymer Bulletin*, vol. 7, pp. 1–7, 2019.

[18] A. Jamil, O. P. Ching, and A. M. Shariff, "Mixed matrix hollow fibre membrane comprising polyetherimide and modified montmorillonite with improved filler dispersion and CO_2/CH_4 separation performance," *Applied Clay Science*, vol. 143, pp. 115–124, 2017.

[19] A. K. Zulhairun and A. F. Ismail, "The role of layered silicate loadings and their dispersion states on the gas separation performance of mixed matrix membrane," *Journal of Membrane Science*, vol. 468, pp. 20–30, 2014.

[20] H. C. Koh, J. S. Park, M. A. Jeong et al., "Preparation and gas permeation properties of biodegradable polymer/layered silicate nanocomposite membranes," *Desalination*, vol. 233, no. 1-3, pp. 201–209, 2008.

[21] H. Abdul Mannan, T. M. Yih, R. Nasir, H. Muhktar, and D. F. Mohshim, "Fabrication and characterization of polyetherimide/polyvinyl acetate polymer blend membranes for CO_2/CH_4

separation," *Polymer Engineering & Science*, vol. 59, no. S1, pp. 293–301, 2019.

[22] A. Jamil, O. P. Ching, and A. M. Shariff, "Minimizing morphological defects of PEI hollow fibre membrane by optimizing the dope viscosity," *ARPN Journal of Engineering and Applied Science*, vol. 11, no. 3, pp. 1687–1690, 2016.

[23] A. F. Ismail and P. Y. Lai, "Effects of phase inversion and rheological factors on formation of defect-free and ultrathin-skinned asymmetric polysulfone membranes for gas separation," *Separation and Purification Technology*, vol. 33, no. 2, pp. 127–143, 2003.

[24] H. Sanaeepur, A. Kargari, and B. Nasernejad, "Aminosilane-functionalization of a nanoporous Y-type zeolite for application in a cellulose acetate based mixed matrix membrane for CO2 separation," *RSC Advances*, vol. 4, no. 109, pp. 63966–63976, 2014.

[25] H. Sanaeepur, A. Kargari, B. Nasernejad, A. E. Amooghin, and M. Omidkhah, "A novel CO_2^+ exchanged zeolite Y/cellulose acetate mixed matrix membrane for CO_2/N_2 separation," *Journal of the Taiwan Institute of Chemical Engineers*, vol. 60, pp. 403–413, 2016.

[26] M. Najafi, M. Sadeghi, A. Bolverdi, M. Pourafshari Chenar, and M. Pakizeh, "Gas permeation properties of cellulose acetate/silica nanocomposite membrane," *Advances in Polymer Technology*, vol. 37, no. 6, 2052 pages, 2018.

[27] H. A. Mannan, H. Mukhtar, T. Murugesan, R. Nasir, D. F. Mohshim, and A. Mushtaq, "Recent applications of polymer blends in gas separation membranes," *Chemical Engineering & Technology*, vol. 36, no. 11, pp. 1838–1846, 2013.

[28] C. Y. Liang, P. Uchytil, R. Petrychkovych et al., "A comparison on gas separation between PES (polyethersulfone)/MMT (Na-montmorillonite) and PES/TiO_2 mixed matrix membranes," *Separation and Purification Technology*, vol. 92, pp. 57–63, 2012.

[29] H. Zhu, X. Jie, L. Wang, G. Kang, D. Liu, and Y. Cao, "Effect of MIL-53 on phase inversion and gas separation performance of mixed matrix hollow fiber membranes," *RSC Advances*, vol. 6, no. 73, pp. 69124–69134, 2016.

[30] S. Bandyopadhyay, E. P. Giannelis, and A. J. Hsieh, "Thermal and thermo-mechanical properties of PMMA nanocomposites," *Polymeric Materials Science and Engineering*, vol. 82, pp. 208-209, 2000.

[31] J. M. Herrera-Alonso, Z. Sedláková, and E. Marand, "Gas transport properties of polyacrylate/clay nanocomposites prepared via emulsion polymerization," *Journal of Membrane Science*, vol. 363, no. 1-2, pp. 48–56, 2010.

[32] C. M. Chan, G. Z. Cao, H. Fong, M. Sarikaya, T. Robinson, and L. Nelson, "Nano-indentation and adhesion of sol-gel-derived hard coatings on polyester," *Journal of Materials Research*, vol. 15, no. 1, pp. 148–154, 2000.

[33] S. V. Hainsworth, H. W. Chandler, and T. F. Page, "Analysis of nanoindentation load-displacement loading curves," *Journal of Materials Research*, vol. 11, no. 8, pp. 1987–1995, 1996.

[34] E. M. Mahdi and J. C. Tan, "Mixed-matrix membranes of zeolitic imidazolate framework (ZIF-8)/Matrimid nanocomposite: thermo-mechanical stability and viscoelasticity underpinning membrane separation performance," *Journal of Membrane Science*, vol. 498, pp. 276–290, 2016.

[35] Y. Hang, G. Liu, K. Huang, and W. Jin, "Mechanical properties and interfacial adhesion of composite membranes probed by in-situ nano-indentation/scratch technique," *Journal of Membrane Science*, vol. 494, pp. 205–215, 2015.

[36] B. D. Beake, S. Chen, J. B. Hull, and F. Gao, "Nanoindentation behavior of clay/poly (ethylene oxide) nanocomposites," *Journal of Nanoscience and Nanotechnology*, vol. 2, no. 1, pp. 73–79, 2002.

[37] N. Muruganandam and D. R. Paul, "Gas sorption and transport in miscible blends of tetramethyl bisphenol-A polycarbonate and polystyrene," *Journal of Polymer Science Part B: Polymer Physics*, vol. 25, no. 11, pp. 2315–2329, 1987.

[38] T. Ishigami, K. Amano, A. Fujii et al., "Fouling reduction of reverse osmosis membrane by surface modification via layer-by-layer assembly," *Separation and Purification Technology*, vol. 99, pp. 1–7, 2012.

[39] S. Shahid and K. Nijmeijer, "High pressure gas separation performance of mixed-matrix polymer membranes containing mesoporous Fe (BTC)," *Journal of Membrane Science*, vol. 459, pp. 33–44, 2014.

[40] Å. Nyflött, Y. Petkova-Olsson, E. Moons et al., "Modeling of oxygen permeation through filled polymeric layers for barrier coatings," *Journal of Applied Polymer Science*, vol. 134, no. 20, p. 44834, 2017.

[41] M. Mubashir, Y. Y. Fong, C. T. Leng, and L. K. Keong, "Prediction of CO2 permeability in NH2-MIL-53 (Al)/cellulose acetate mixed matrix membranes using theoretical models," *International Journal of Integrated Engineering*, vol. 10, no. 5, p. 176, 2018.

[42] M. Behroozi and M. Pakizeh, "Study the effects of Cloisite15A nanoclay incorporation on the morphology and gas permeation properties of Pebax2533 polymer," *Journal of Applied Polymer Science*, vol. 134, no. 37, p. 45302, 2017.

[43] B. Freeman, Y. Yampolskii, and I. Pinnau, *Materials Science of Membranes for Gas and Vapor Separation*, John Wiley & Sons, 2006.

[44] H. Lin and B. D. Freeman, "Gas solubility, diffusivity and permeability in poly (ethylene oxide)," *Journal of Membrane Science*, vol. 239, no. 1, pp. 105–117, 2004.

[45] E. Picard, A. Vermogen, E. Picard, A. Vermogen, J. F. Gérard, and E. Espuche, "Barrier properties of nylon 6-montmorillonite nanocomposite membranes prepared by melt blending: influence of the clay content and dispersion state consequences on modelling," *Journal of Membrane Science*, vol. 292, no. 1-2, pp. 133–144, 2007.

[46] J. H. Kim and Y. M. Lee, "Gas permeation properties of poly (amide-6-b-ethylene oxide)–silica hybrid membranes," *Journal of Membrane Science*, vol. 193, no. 2, pp. 209–225, 2001.

[47] K. Kalantari, P. Moradihamedani, N. A. Ibrahim, A. H. Abdullah, and A. B. Afifi, "Polysulfone mixed-matrix membrane incorporating talc clay particles for gas separation," *Polymer Bulletin*, vol. 75, no. 8, pp. 3723–3738, 2018.

[48] A. Jamil, O. P. Ching, and A. B. Shariff, "Polyetherimide-montmorillonite mixed matrix hollow fibre membranes: effect of inorganic/organic montmorillonite on CO_2/CH_4 separation," *Separation and Purification Technology*, vol. 206, pp. 256–267, 2018.